ACS APPLIED MATERIALS & INTERFACES

Research Article

www.acsami.org

Molecular Composition, Grafting Density and Film Area Affect the Swelling-Induced Au−S Bond Breakage

Bei'er Lv,[†,‡] Yitian Zhou,[†] Wenli Cha,[†] Yuanzi Wu,[†] Jinxing Hu,[†] Liqiang Li,[§] Lifeng Chi,[§] and Hongwei Ma*[,†]

[†]Division of Nanobiomedicine, Suzhou Institute of Nano-Tech and Nano-Bionics, Chinese Academy of Sciences, Suzhou 215123, People's Republic of China

[‡]University of Chinese Academy of Sciences, Beijing 100049, People's Republic of China

[§]Physikalisches Institut and Center for Nanotechnology (CeNTech), Universität Münster, 48149 Münster, Germany

Supporting Information

ABSTRACT: In previous studies, we reported the first observation of the Au−S bond breakage induced mechanically by the swelling of the surface-tethered weak polyelectrolyte brushes in phosphate buffered saline (PBS), a phenomenon with broad applications in the fields of biosensors and functional surfaces. In this study, three factors, namely the molecular composition, grafting density and film area of the weak polyelectrolyte, carboxylated poly(oligo(ethylene glycol) methacrylate-random-2-hydroxyethyl methacrylate) (poly(OEGMA-r-HEMA)), were studied systematically on how they affected the swelling-induced Au−S bond breakage (ABB). The results showed that, first, the swelling-induced ABB is applicable to a range of molecular compositions and grafting densities; but the critical thickness ($T_{critical,dry}$) varied with both of the two factors. An analysis on the swelling ratio further revealed that the difference in the $T_{critical,dry}$ arose from the difference in the swelling ability. A film needed to swell to ~250 nm to induce ABB regardless of its composition or structure, thus a higher swelling ratio would lead to a lower $T_{critical,dry}$ value. Then, the impact of the film area was studied in micrometer- and sub-micrometer-scale brush patterns, which showed that only partial, rather than complete ABB was induced in these microscopic films, resulting in buckling instead of film detaching. These results demonstrated that the ABB is suitable to be used in the design of biosensors, stimulus-responsive materials and mechanochemical devices. Although the >160 μm^2 required area for uniform ABB hinders the application of ABB in nanolithography, the irreversible buckling provides a facile method of generating rough surfaces.

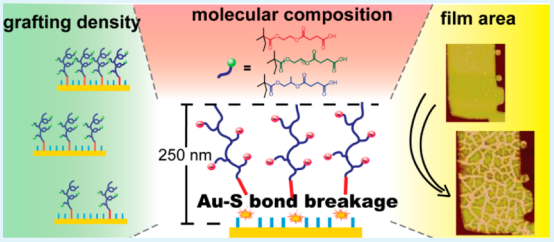

KEYWORDS: *polymer brush, swelling behavior, Au−S bond, functional surface, mechanochemistry, surface buckling*

INTRODUCTION

The controllable swelling behavior of surface-tethered polymer brushes in liquids has been exploited for the rational design of nanoactuators,[1−3] drug delivery systems,[4−6] biosensors,[7−9] microfluidic devices[10,11] and other functional surfaces.[12−14] Swelling is the result of chain extension that is caused by short-range chain repulsion or short/long-range electrostatic interactions, or a combination of both.[15] The degree of swelling is usually evaluated by the "swelling ratio", which is the ratio of the film thickness in a certain liquid to that in dry state. Among the three categories of the polymer brushes, namely neutral, weak and strong polyelectrolyte brushes, the swelling behavior of weak polyelectrolytes is the most complicated, because it is the only situation in which the degree of charging of the grafted chains is subject to changing.[16] This, however, actually imparts it with the potential of fine regulation.

Although most applications focused on the reversible conformational shift during swelling, we also took use of the stress generated within the brushes to break specific covalent bond,[17] so as to bring in one more dimension of regulation. Triggering chemical reactions with mechanical force (often by ultrasonic processing, grinding or single-molecular force spectroscopy), the mechanochemisty, possesses certain advantages in that it often could be proceeded in mild or even ambient conditions, and that it enables the reactions to be directed along pathways that may not be conventionally obtainable through heat, light or electric stimuli.[18−20] As an initial proof of concept, the selective breakdown of Au−S bond has been shown to be induced by the swelling of weak polyelectrolyte brush, the carboxylated poly(oligo(ethylene glycol) methacrylate-random-2-hydroxyethyl methacrylate) (hereafter abbreviated as carboxylated poly(OEGMA-r-HEMA)), which was anchored at one end on a gold surface via the Au−S bonds[17] (Scheme 1). Although the instability of Au−S bonds has been common knowledge,[21] the degradation of Au−S bond usually still requires harsh treatments.[22] However, in the mechanochemical regime, it was broken immediately by contact with the phosphate buffered saline

Received: February 24, 2014
Accepted: May 6, 2014
Published: May 6, 2014

   dx.doi.org/10.1021/am501150m | ACS Appl. Mater. Interfaces 2014, 6, 8313−8319

Scheme 1. Preparation of Carboxylated Poly(OEGMA-r-HEMA) from Gold Surface and the Swelling-Induced Au−S Bond Breakage

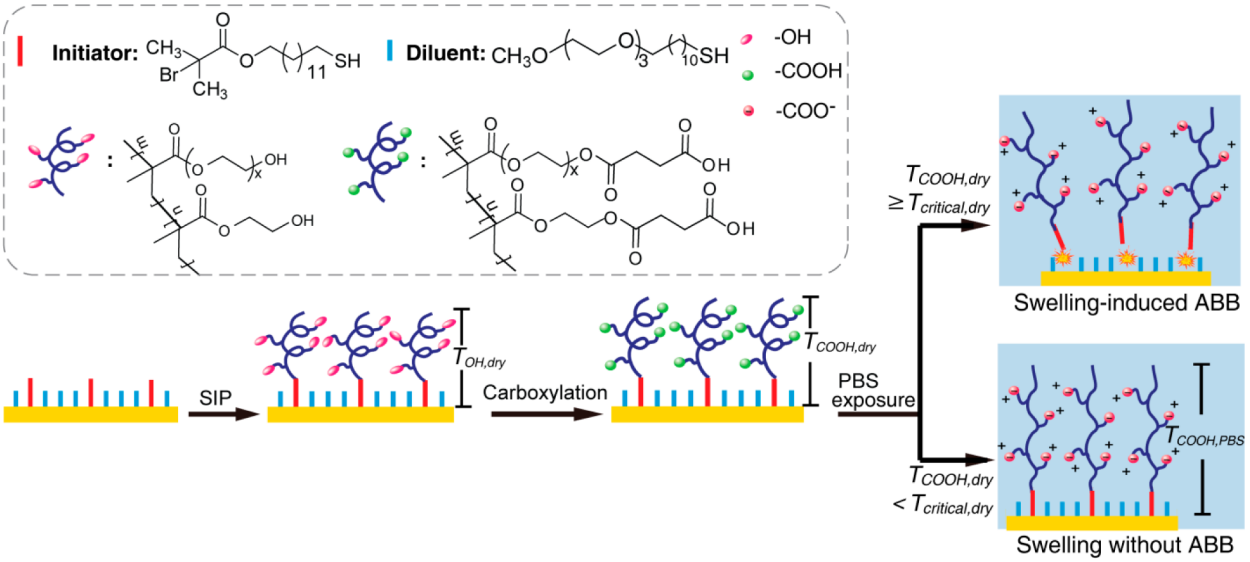

(PBS) in ambient environment. The degradation of Au−S bonds led to complete detachment of the brush film, which could be monitored by the quartz crystal microbalance (QCM) in real time and has been characterized by the scanning electron microscopy (SEM) and atomic force microscopy (AFM).[17]

Such swelling-induced Au−S bond breakage (ABB) had been found to depend on the film thickness: only films with dry thicknesses surpassing a certain value could induce ABB, which was defined as the critical dry thickness ($T_{critical,dry}$).[17,23] In the previous studies,[24] for the carboxylated poly(OEGMA-r-HEMA) films of two different monomer molar ratios (with OEGMA:HEMA being 0.25:0.75 and 0.48:0.52), the $T_{critical,dry}$ values were determined and found to differ significantly (57 and 75 nm, respectively). However, multiplying each $T_{critical,dry}$ with corresponding swelling ratio gave birth to two very close values (236 and 249 nm, respectively), which suggested that it is the wet thickness of a swollen film that directly dictates whether or not ABB would happen. A ∼250 nm thick swollen film might provide the force required for Au−S bond degradation and thus triggers ABB.

These previous studies only focused on weak polyelectrolytes of one single grafting density and chemical composition. However, a systematic analysis on the effect of grafting density and chemical composition is the prerequisite for both the understanding and application of ABB. In the design of smart bioactive surfaces, the grafting density and chemical composition of polymer brushes are routinely tuned to achieve optimal outcome in a balance of conjugation efficiency, antifouling property and stimulus-responsiveness.[9,25] Therefore, examining whether ABB is compatible with other grafting densities and composition is critical for its application in that field. Another key question is the following: for ABB of all these diverse structure and composition, will the 250 nm wet-thickness remain the universal dictating factor? The answer of this question will determine, to a large part, whether swelling holds the potential of becoming a mature treatment for mechanochemistry.

Therefore, in this current study, we address these questions by first examining the ABB property of carboxylated poly(OEGMA-r-HEMA) of a series of grafting densities, and then investigating other weak polyelectrolytes with different molecular compositions, with particular attention to the analysis of $T_{critical,dry}$ and its relation with swelling ability. In addition, the effect of film area on ABB was studied on a range of micrometer- and sub-micrometer-scale carboxylated poly(OEGMA-r-HEMA) patterns obtained with the aid of electron beam lithography.

EXPERIMENTAL SECTION

Preparation of the Surface-Tethered Polyelectrolytes. All the weak polyelectrolytes used in this work were carboxylated poly(OEGMA-r-HEMA) unless otherwise indicated. Carboxylated poly(OEGMA-r-HEMA) brushes were prepared as described previously[9] (Scheme 1). First, a quartz crystal microbalance (QCM) chip (AT cut, 5 MHz; HZDW, Hangzhou, China) or gold-deposited silicon wafer was modified with the binary self-assembled monolayers (SAMs) composed of the initiator thiol (ω-mercaptoundecyl bromoisobutyrate) and the diluent thiol ((11-mercaptoundecyl)tri(ethylene glycol)), by incubating in the ethanol solution for 14 h at room temperature (rt) and protection from light. The sum of the concentration of initiator and diluent in the solution was kept at 1 mM while the ratio between the two was tuned to control the grafting density as described in the following. Second, the neutral polymer brush of poly(OEGMA-r-HEMA) was synthesized via surface-initiated atom transfer radical polymerization (SI-ATRP) from the initiator-modified surfaces. In this step, bipyridine was adopted as the ligand and water:ethanol = 1:1 as the solvent (the water used in this work was Milli-Q water with resistivity of 18.2 MΩ cm^{-1}), with a molar ratio of OEGMA/HEMA/$CuCl_2$/bipyridine/ascorbic acid = 125/125/1/2/1 (i.e., 500/500/4/8/4 mM). "OEGMA" refers to the OEGMA monomer with M_n = 526 hereafter unless otherwise indicated. The reaction mixture was degassed with argon for 1 h before moved into a glovebox for SI-ATRP. The reaction was terminated with Milli-Q water, and the chips were then rinsed thoroughly with Milli-Q water and ethanol and dried under a nitrogen flow.

Finally, weak polyelectrolyte brushes were produced by converting the hydroxyl ends of poly(OEGMA-r-HEMA) to carboxyl groups. Poly(OEGMA-r-HEMA) grafted chips were immersed in a *N,N*-dimethylformamide (DMF) solution containing succinic anhydride (10 mg mL^{-1}) and 4-(dimethylamino) pyridine (15 mg mL^{-1}) for 8 h at rt. The chips were then rinsed with DMF and methanol thoroughly to remove any salt particles and dried under a nitrogen flow.

dx.doi.org/10.1021/am501150m | ACS Appl. Mater. Interfaces 2014, 6, 8313−8319

The grafting density was tuned by controlling the initiator density χ_I ($\chi_I = n_{initiator}/(n_{initiator} + n_{diluent})$ of the SAM solutions. Five groups of carboxylated poly(OEGMA-r-HEMA) were synthesized in the first section of the Results and Discussion, with χ_I being 2.5%, 5%, 7.5%, 10% and 100%, respectively. χ_I was fixed at 2.5% in the other sections.

For the copolymerization of other monomers, the above procedure was followed with the same monomer ratio (1:1) unless otherwise indicated; for homopolymerization, a ratio of monomer/$CuCl_2$/bipyridine/ascorbic acid = 250/1/2/1 were used. The monomers of hydroxypropyl methacrylate and the OEGMA (M_n = 360) are hereafter abbreviated as HPMA and $OEGMA_{360}$, respectively.

Surface Characterizations. The thickness of the dry and wet films that tethered on the QCM chips were calculated from QCM data with the Sauerbrey equation and "solidified liquid layer" model, respectively, as reported previously.[9,26] In the third section of the Results and Discussion, the dry thicknesses of the laterally infinite controls that tethered on the gold coated silicon wafers were measured by ellipsometry. The area and dry thickness of the micrometer-scale brush patterns were determined by atomic force microscopy (AFM).

The ellipsometry measurement was performed on an M-2000V spectroscopic ellipsometer (J.A. Woollam Co., Inc.) at angles of 65°, 70° and 75° and wavelengths from 400 to 800 nm. Ellipsometric data were fitted for thickness with the material-specific model (Cauchy layer model) from a vendor-supplied software, with fixed (An, Bn) values (1.46, 0.01).

All of the AFM images were obtained in the tapping mode using a Veeco Dimension 3100 (Digital Instruments, Santa Barbara) in air at rt. The thickness and roughness were analyzed by the "Step" and "Roughness" functions in the vendor-supplied software.

ABB Test. The swelling and swelling-induced ABB in PBS (pH = 7.4, $[Na^+]$ = 150 mM) were monitored in real time by liquid phase QCM measurement. A home-built QCM was used with control software purchased from Resonant Probes GmbH (Goslar, Germany). Water or PBS was pumped through by a peristaltic pump at a speed of 80 μL min^{-1} and the change in frequency and dissipation were recorded in real time. The PBS solution was prepared as the following: 8.00 g of NaCl, 0.20 g of KCl, 0.24 g of KH_2PO_4, 3.63 g of $Na_2HPO_4 \cdot 12H_2O$ were dissolved into 1 L of water.

RESULTS AND DISCUSSION

Effect of Grafting Density on ABB. Neutral poly(OEGMA-r-HEMA) films were prepared via surface-initiated polymerization (SIP) from the gold surface of QCM chips immobilized with a self-assembled monolayer (SAM) of initiators and diluents (Scheme 1). Conversion of hydroxyl ends to carboxyl-ended groups with succinic anhydride gave rise to weak polyelectrolyte−carboxylated poly(OEGMA-r-HEMA).

The grafting density was controlled by varying the molar ratio between the initiator and diluent in the solution for self-assembling. The initiator density, χ_I, was defined as the solution initiator density ($\chi_I = n_{initiator}/(n_{initiator} + n_{diluent})$). Because the surface initiator density is proportional to the solution initiator density, and it has been suggested that in the case of sparse grafting the grafting density is in proportional with the surface initiator density, we adopted χ_I as an indicator of grafting density.[9] In previous studies, the χ_I was fixed at 2.5%; in this study, five χ_Is were used: 2.5%, 5%, 7.5%, 10% and 100%.

The dry thicknesses of the polymer films before and after carboxylation were designated as $T_{OH,dry}$ and $T_{COOH,dry}$ (Scheme 1). Therefore, the values of $T_{OH,dry}$ were used to analyse the SIP kinetics. For all five χ_Is, the linear increase of $T_{OH,dry}$ lasted for less than 5 h when growth started to slow down (Figure 1a), consistent with previous results.[27]

Next the relation between χ_I and grafting density was checked (Figure 1b): for a given polymerization time (within 8 h), the film thickness showed a linear relationship with χ_I in the range from 2.5% to 7.5% and the linear fitting started to deviate from 10%, which suggested that only in the range between 2.5% and 7.5% could the χ_I confidently represent the chain density.[9] When χ_I reached 10%, it was no longer in proportional with the grafting density due to steric hindrance.

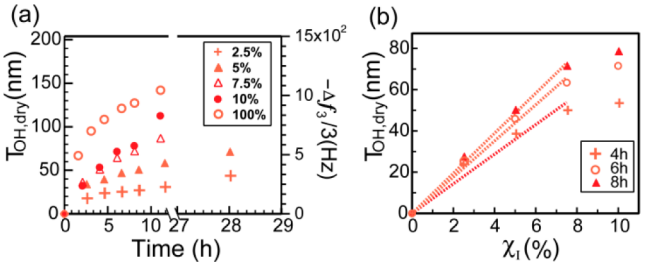

Figure 1. Surface-initiated polymerization of poly(OEGMA-r-HEMA) from mixed SAMs of initiator and diluent under the five initiator densities. (a) The growth of $T_{OH,dry}$ with time; (b) A linear relation between $T_{OH,dry}$ and χ_I was observed within the range 2.5% ≤ χ_I ≤ 7.5% for a given SIP duration (4, 6, and 8 h).

After carboxylation, the films were subjected to the ABB test, in which the PBS treatment was monitored by QCM to distinguish two types of responses: only swelling ($T_{COOH,dry} < T_{critical,dry}$), or swelling-induced Au−S bond breakage ($T_{COOH,dry} \geq T_{critical,dry}$). Upon the distinguishing of the two, the $T_{critical,dry}$ of each χ_I group was determined. ABB was observed on films of all the five χ_Is, which induced a frequency response in virtually the same fashion (Figure 2), but the $T_{critical,dry}$ values varied

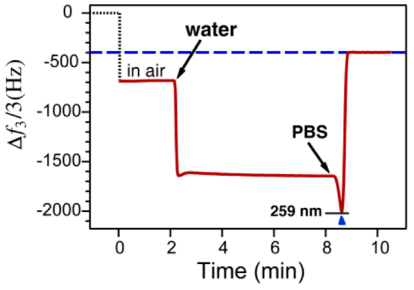

Figure 2. Time course of ABB of a carboxylated poly(OEGMA-r-HEMA) film (χ_I = 2.5%, $T_{COOH,dry}$ = 89 nm) as monitored by QCM. It shows the typical response of QCM frequency to ABB. A decrease in $\Delta f_3/3$ after the introduction of water or PBS corresponded to an increase in film thickness (the swelling). Then, a sudden increase in $\Delta f_3/3$ corresponded to the detachment of the film induced by ABB. The blue arrow designated the starting point of ABB, where the wet thickness was 259 nm. The blue dashed line designated the level corresponding to a bared chip in PBS ($\Delta f_3/3$ = −400 Hz).

(Figure 3b). We then investigated the swelling ratios to examine whether the difference in $T_{critical,dry}$ arose from the variation in swelling ability.

The swelling ratio in PBS (t_{PBS}) was defined as the ratio of the wet film thickness in PBS ($T_{COOH,PBS}$) to $T_{COOH,dry}$ ($t_{PBS} = T_{COOH,PBS}/T_{COOH,dry}$). It had been observed that films with the same χ_I but different thickness showed the same value of t_{PBS}.[23] Therefore, the t_{PBS} of each group of χ_I was determined as the following: first, for each group of χ_I, the wet thickness ($T_{COOH,PBS}$) of each film, which only swelled but did not induce ABB in PBS ($T_{COOH,dry} < T_{critical,dry}$), was calculated from QCM data with the "solidified liquid layer" model.[26] Then the $T_{COOH,PBS}$ values were plotted against the $T_{COOH,dry}$ values to

dx.doi.org/10.1021/am501150m | ACS Appl. Mater. Interfaces 2014, 6, 8313−8319

(a)

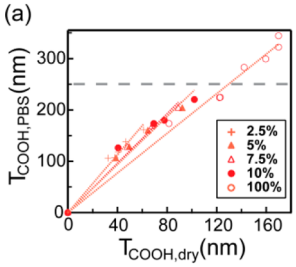

(b)

χ_I	$T_{critical,dry}$ (nm)	t_{PBS}	Theoretical $T_{critical,dry}$ (nm)
2.5%	80	2.83	88
5%	94~110	2.36	106
7.5%	90~105	2.41	104
10%	102~109	2.34	107
100%	155*	1.93	130

Figure 3. Effect of initiator density on the swelling ratio and ABB property. (a) $T_{COOH,PBS}$ was plotted against $T_{COOH,dry}$ to fit for swelling ratios. The black dash line represent the level of $T_{COOH,PBS}$ = 250 nm. (Fitting was forced to pass (0, 0) point; $n \geq 4$ and all $R^2 > 0.95$.) (b) Comparison of swelling ratio and the experimental and theoretical critical dry thickness among the five χ_I values. The asterisk indicates that not all the 100% films that met this $T_{critical,dry}$ underwent ABB, whereas those of other χ_I values did.

linearly fit for t_{PBS} (Figure 3a). A general trend was observed (Figure 3a,b) that the t_{PBS} decreased with the χ_I in the whole range (from 2.5% to 100%), but there was no statistic difference among $t_{PBS,5\%}$, $t_{PBS,7.5\%}$ and $t_{PBS,10\%}$ ($F_{2,9}$ = 0.040, $P > 0.05$, one-way analysis of variance (ANOVA) test). The decrease in t_{PBS} was an effect of chain density rather than the insufficiency in carboxylation (please refer to section 2.2 of the Supporting Information for detailed discussion).

It is not difficult to note the opposite trends between the changing of t_{PBS} and $T_{critical,dry}$, a reminiscence of the relation between the two among films of the same χ_I but different monomer ratios.[24] Thus, we further assumed that the 250 nm of wet thickness of a swollen film remains a cross-chain-density factor that dictates whether ABB could happen and calculated the "theoretical $T_{critical,dry}$" by 250 nm/t_{PBS} (Figure 3b). The theoretical and experimental values virtually agreed well, hence verifying the assumption.

It is interesting that the force generated via swelling is only dependent on film thickness but independent of the film structure. However, for the 100% group, there was still a notable deviation between theoretical and experimental $T_{critical,dry}$. In particular, of the five 100% films that swelled to thickness higher than 250 nm, only one triggered ABB (the other four were shown as points above the black dashed line in Figure 3a). As it is known that in the case of 100% initiator density, polymerization was affected heavily by bimolecular termination,[27] resulting in higher polydispersity in chain length, we maintain that it was the higher heterogeneity in main chain structure that was responsible for the notable disinclination for ABB. Therefore, ABB is also influenced by the homogeneity in film structure.

Note that although the $T_{critical,dry}$ of swelling-induced ABB increases with χ_I as a general trend, it was very close in the range of χ_I from 5% to 10% and moderately close from 2.5% to 10%. Therefore, a concept of "global critical dry thickness" could be raised, $T_{critical,dry,gb}$ = 110 nm, which means synthesizing a film that reaches 110 nm could guarantee ABB, with any initiator density in that range. This conclusion provides valuable information for applying the swelling-induced ABB for biosurface design.

Effect of Molecular Composition on ABB. To investigate the effect of molecular composition on the swelling-induced Au−S bond breakage, several relevant vinyl monomers were chosen to synthesize homo- and co-polyelectrolytes other than the carboxylated poly(OEGMA$_{526}$-r-HEMA):carboxylated poly(OEGMA$_{526}$), poly(HEMA), poly(OEGMA$_{526}$-r-HPMA) and poly(OEGMA$_{526}$-r-OGEMA$_{360}$) with initiator density fixed at 2.5% (the subscript refers to the number-averaged molecular weight of OEGMA). These surface-tethered weak polyelectrolytes were then subject to ABB test.

For the homopolymers carboxylated poly(OEGMA$_{526}$) and poly(HEMA), none of the films induced ABB after PBS incubation even for those with dry film thickness as high as 123 and 197 nm, respectively (Table 1). In contrast, carboxylated poly(OEGMA$_{526}$-r-HPMA) and poly(OEGMA$_{526}$-r-OEGMA$_{360}$) exhibit growth rates that were similar to carboxylated poly(OEGMA$_{526}$-r-HEMA) and both were amenable to ABB, with $T_{critical,dry}$ being 90 and 60 nm, respectively (Table 1). Again, the difference among the three polyelectrolytes in $T_{critical,dry}$ stemmed from their difference in swelling ratio, because multiplying $T_{critical,dry}$ by t_{PBS} greatly offset the difference, giving rise to values close to 250 nm (Table 1). This implied that the wet thickness of 250 nm was also the decisive factor for the ABB of these copolymers with different monomer type. Therefore, we define it as the "critical wet thickness" ($T_{critical,wet}$) of ABB.

Table 1. Comparison of Swelling Ratio of Surface-Tethered Carboxylated Poly(OEGMA$_{526}$), Poly(HEMA), Poly(OEGMA$_{526}$-r-OEGMA$_{360}$) and Poly(OEGMA$_{526}$-r-HPMA) and the Corresponding ABB Properties

polyelectrolyte type	t_{PBS}[a]	$T_{critical,dry}$ (nm)	$t_{PBS} \times T_{critical,dry}$ (nm)
carboxylated poly(OEGMA$_{526}$)	2.62		
carboxylated Poly(HEMA)	5.93		
carboxylated poly(OEGMA$_{526}$-r-OEGMA$_{360}$)	4.00	60	240
carboxylated poly(OEGMA$_{526}$-r-HPMA)	2.84	90	256

[a]The swelling ratios were determined by linearly fitting with $R^2 > 0.95$ (fitting was forced to pass (0,0) point) and by our previous studies[24] (Figures S3 and S4, Supporting Information).

The results obtained in these two sections demonstrated that (1) the swelling-induced ABB is not limited to surface-tethered carboxylated poly(OEGMA$_{526}$-r-HEMA) with χ_I = 2.5%, proving its potential use in the design of functional surfaces; (2) the magnitude of force generated by swelling of the copolymers is determined only by wet film thickness, independent of chemical composition or chain density, suggesting its application in mechanochemistry; (3) the disinclination for ABB in the case of χ_I = 100% and homopolymers implied that ABB also relies on the microstructure of a film besides its wet thickness. ABB might require homogeneity in the main chain structure but heterogeneity in side chains.

Influence of Film Area on ABB. The ABB leads to the complete detachment of surface-tethered brushes and re-exposure of gold surface, which suggested that it might also be regarded as a form of aqueous etching that could be utilized for surface patterning with the aid of masks or by being integrated into dip-pen nano/micro lithography[28,29] (Scheme S1. Supporting Information). Spatial resolution is key to micro/nano fabrications. The resolution would then be determined by the minimum film area required to induce ABB. Therefore, in this section, we investigated the influence of film area on ABB to evaluate whether ABB is suitable for that application.

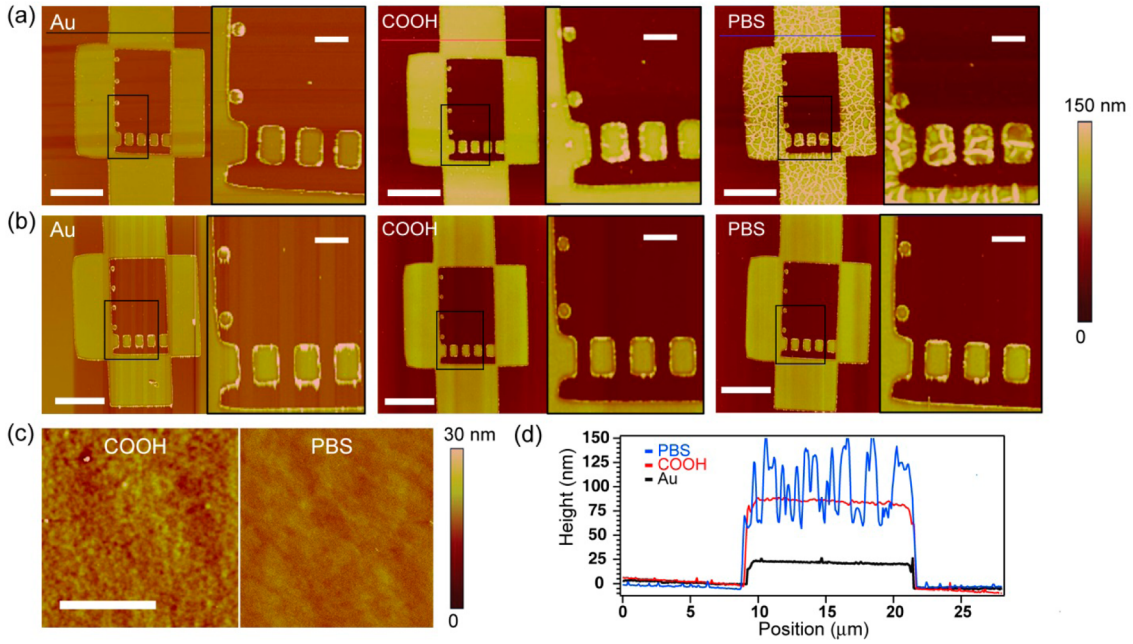

Figure 4. ABB gave rise to buckling morphology instead of film detachment in the micrometer-scale patterns. (a, b) AFM height graph of the microscale gold surface (Au), carboxylated poly(OEGMA-r-HEMA) grafted surface (COOH), and PBS-treated surface (PBS) of one pattern unit of Group 1 (a) and Group 3 (b), respectively. In each section, the right image is an enlarged view of the region framed by a black box in the left image; the scale bar of the left and right image represents for 10 μm and 2 μm, respectively, for all six sections of panels a and b. (c) The surface morphology before (left) and after (right) ABB of one macroscale control of Group 1. Scale bar = 5 μm. (d) Height information as sectioned along the black/red/blue line of the "Au", "COOH" and "PBS" section in panel a, respectively. All AFM graphs were obtained in air at room temperature.

Using electron beam exposure and metal evaporation, patterns of microscopic gold surfaces were deposited on a silicon substrate, so that every unit contained gold patterns ranging from micrometer down to sub-micrometer scale (Figure 4a): two 10 × 10 μm^2, two 8 × 20 μm^2, three 1.5 × 2.5 μm^2 and four 0.8 × 0.8 μm^2 microstructures. Then SIP and carboxylation on the gold surfaces gave rise to patterned carboxylated poly(OEGMA-r-HEMA) brushes (χ_I = 2.5%).

By tuning the SIP duration, three groups of polyelectrolyte pattern units that differed only in film thickness were obtained, one above $T_{critical,dry}$[30] (Group 1: 62.4 ± 3.6 nm), one slightly below the $T_{critical,dry}$ (Group 2: 48.2 ± 7.5 nm), and one far below the $T_{critical,dry}$ (Group 3: 38.4 ± 3.0 nm). Each group contained six units. In addition, the macroscopic-scale controls, the laterally infinite polyelectrolyte brushes that tethered on 8 × 8 mm^2 gold surfaces, were also prepared for each group, with all other conditions kept the same (Table S2, Supporting Information).

The micrometer-scale patterns and macroscale controls of each group were then immersed in PBS for 24 h. AFM was applied to characterize the morphological changes. As expected, ABB occurred to the macroscale controls of Group 1, causing the films to detach completely (Figure 4c). The microscale patterns of Group 1, however, stayed adhered to the surface after the same period of exposure (for all of the 6 units under investigation, Figure 4a). However, while not detaching, the patterned brushes underwent significant morphological changes, buckling out of the pristine smooth surfaces (Figure 4a,d). Although buckling of nanofilms is a known phenomenon that is caused by partial bond degradation,[31,32] this is the first time that a buckling morphology is observed in the ABB condition. This result suggested that partial ABB has been induced during the exposure to PBS, but uniform, complete ABB was hindered by the confined film area.

The macroscale controls of Group 2 and 3 underwent no change after PBS treatment as expected. As for the patterned units, all of the 6 units of Group 3, as well as 3 of the 6 units of Group 2, showed no notable change (Figure 4b), neither detaching nor buckling, but the remaining 3 units of Group 2 underwent slight buckling on the up-micrometer-scale regions (Figure S5, Supporting Information). These results were consistent with our explanation: Group 3 did not undergo ABB because their thicknesses were far below $T_{critical,dry}$; half of Group 2 underwent partial ABB in sparse regions for their thickness was just slightly below the critical dry thickness.

It could be concluded from these results that the uniform ABB (i.e., the complete detachment) relied on film area, with the 160 μm^2 regions, the largest in this study, only triggering partial ABB. In previous experiments, we have observed that the detached brushes existed in the form of thin fibers of 50−100 μm thick and one or several millimeters long that were visible to the naked eye, consistent with the results presented here. While the reason for the area requirement is currently not clear, we suggest that the ABB is not suitable for applications demanding lateral resolution such as the dip-pen lithography. The area requirement might be dictated by the property of the physical cross-linking of the brush chains and studies are currently underway to investigate larger sizes.

The buckling results implied that, during ABB, the film kept intact, rather than left the surface one brush after another, consistent with the findings reported by others that polymer brushes, even not chemically cross-linked, tended to stay as a membrane, and to fold, wrinkle or buckle rather than tear or fracture under HF etching.[12] The ridges were representations of the lateral swelling of the film, as evidenced by the roughness analysis data, which showed that although the size and height of the ridging patterns differed among units, the "surface area

difference" was fixed at around 3% (Figure S6, Supporting Information).

The >160 μm^2 required area for complete ABB suggests it is not suitable for nanolithography. However, as a novel approach to producing buckled surface, which is convenient compared with other strategies, the swelling-induced ABB may find use in the creation of rough surface for the study of cell adhesion and other functional applications.[31,32] In contrast with the buckling of the "polymer carpets" created by Amin et al.,[33] the buckling induced here was not reversible, also an indication of only partial Au−S breakage.

CONCLUSIONS

In summary, the swelling-induced ABB was proved to be applicable to weak polyelectrolytes of a range of molecular compositions and grafting densities, but hindered in homopolymers and in the case of 100% initiator density. The critical wet thickness ($T_{critical,wet} \approx 250$ nm) was proved the universal decisive parameter for ABB independent of composition and chain density. The influence of molecular composition and chain density on ABB were determined by their influences on swelling ratio. The film area affected ABB: on the micrometer-scale brush patterns, partial ABB gave rise to intriguing buckling morphology instead of film detachment. These results demonstrated the universality and tunability of the swelling-induced ABB, which is critical for its application in the development of biosensors, functional surfaces and mechano-chemical systems. Effort is currently underway to (1) construct a model to explain the mechanism of ABB, (2) further confirm and characterize the breakage of Au−S bonds in this process and (3) realize the application of ABB.

ASSOCIATED CONTENT

Supporting Information

A conceptual design of applying ABB for micro/nano-lithography (Scheme S1), the uncontrollable thickness growth after 15 h (Figure S1), the calculation of carboxyl density (section 2.2 of the Supporting Information), the detailed calculation of swelling ratios of films with different composition (Figures S3 and S4), the thickness of macroscale control films (Table S2), the buckling of Group 2 (Figure S5) and the roughness parameters of the buckling of Group 1 (Figure S6). This material is available free of charge via the Internet at http://pubs.acs.org.

AUTHOR INFORMATION

Corresponding Author

*H. Ma. E-mail: hwma2008@sinano.ac.cn.

Notes

The authors declare no competing financial interest.

ACKNOWLEDGMENTS

This work was supported by the Chinese Academy of Sciences (KJZD-EW-J01) and NSFC (21174161) to H. Ma. The authors are grateful to Dr. Yanxia Zhang for discussion on the paper.

REFERENCES

(1) Zhou, F.; Biesheuvel, P. M.; Choi, E.-Y.; Shu, W.; Poetes, R.; Steiner, U.; Huck, W. T. S. Polyelectrolyte Brush Amplified Electroactuation of Microcantilevers. *Nano Lett.* **2008**, *8*, 725−730.

(2) Comrie, J. E.; Huck, W. T. S. Exploring Actuation and Mechanotransduction Properties of Polymer Brushes. *Macromol. Rapid Commun.* **2008**, *29*, 539−546.

(3) Chen, T.; Chang, D. P.; Zhang, J.; Jordan, R.; Zauscher, S. Manipulating the Motion of Gold Aggregates Using Stimulus-Responsive Patterned Polymer Brushes as a Motor. *Adv. Funct. Mater.* **2012**, *22*, 429−434.

(4) Yang, Y. Q.; Guo, X. D.; Lin, W. J.; Zhang, L. J.; Zhang, C. Y.; Qian, Y. Amphiphilic Copolymer Brush with Random PH-Sensitive/Hydrophobic Structure: Synthesis and Self-Assembled Micelles for Sustained Drug Delivery. *Soft Matter* **2012**, *8*, 454−464.

(5) Motornov, M.; Tam, T. K.; Pita, M.; Tokarev, I.; Katz, E.; Minko, S. Switchable Selectivity for Gating Ion Transport with Mixed Polyelectrolyte Brushes: Approaching "Smart" Drug Delivery Systems. *Nanotechnology* **2009**, *20*, 434006.

(6) Kiser, P. F.; Wilson, G.; Needham, D. A Synthetic Mimic of the Secretory Granule for Drug Delivery. *Nature* **1998**, *394*, 459−462.

(7) Zhang, Y.; Islam, N.; Carbonell, R. G.; Rojas, O. J. Specific Binding of Immunoglobulin G with Bioactive Short Peptides Supported on Antifouling Copolymer Layers for Detection in Quartz Crystal Microgravimetry and Surface Plasmon Resonance. *Anal. Chem.* **2012**, *85*, 1106−1113.

(8) Welch, M.; Rastogi, A.; Ober, C. Polymer Brushes for Electrochemical Biosensors. *Soft Matter* **2011**, *7*, 297−302.

(9) Ma, H.; He, J. a.; Liu, X.; Gan, J.; Jin, G.; Zhou, J. Surface Initiated Polymerization from Substrates of Low Initiator Density and Its Applications in Biosensors. *ACS Appl. Mater. Interfaces* **2010**, *2*, 3223−3230.

(10) Xu, C.; Fu, X. F.; Fryd, M.; Xu, S.; Wayland, B. B.; Winey, K. I.; Composto, R. J. Reversible Stimuli-Responsive Nanostructures Assembled from Amphiphilic Block Copolymers. *Nano Lett.* **2006**, *6*, 282−287.

(11) Beebe, D. J.; Moore, J. S.; Bauer, J. M.; Yu, Q.; Liu, R. H.; Devadoss, C.; Jo, B.-H. Functional Hydrogel Structures for Autonomous Flow Control inside Microfluidic Channels. *Nature* **2000**, *404*, 588−590.

(12) Welch, M. E.; Ober, C. K. Characterization of Polymer Brush Membranes via HF Etch Liftoff Technique. *ACS Macro Lett.* **2013**, *2*, 241−245.

(13) Peng, S.; Bhushan, B. Smart Polymer Brushes and Their Emerging Applications. *RSC Adv.* **2012**, *2*, 8557−8578.

(14) Barbey, R.; Lavanant, L.; Paripovic, D.; Schuwer, N.; Sugnaux, C.; Tugulu, S.; Klok, H. A. Polymer Brushes via Surface-Initiated Controlled Radical Polymerization: Synthesis, Characterization, Properties, and Applications. *Chem. Rev.* **2009**, *109*, 5437−527.

(15) Borisov, O. V.; Zhulina, E. B.; Birshtein, T. M. Diagram of the States of a Grafted Polyelectrolyte Layer. *Macromolecules* **1994**, *27*, 4795−4803.

(16) Zhulina, E. B.; Birshtein, T. M.; Borisov, O. V. Theory of Ionizable Polymer Brushes. *Macromolecules* **1995**, *28*, 1491−1499.

(17) Zhang, Y.; He, J.; Zhu, Y.; Chen, H.; Ma, H. Directly Observed Au-S Bond Breakage due to Swelling of the Anchored Polyelectrolyte. *Chem. Commun.* **2011**, *47*, 1190−1192.

(18) Hickenboth, C. R.; Moore, J. S.; White, S. R.; Sottos, N. R.; Baudry, J.; Wilson, S. R. Biasing Reaction Pathways with Mechanical Force. *Nature* **2007**, *446*, 423−427.

(19) Brantley, J. N.; Wiggins, K. M.; Bielawski, C. W. Unclicking the Click: Mechanically Facilitated 1,3-Dipolar Cycloreversions. *Science* **2011**, *333*, 1606−1609.

(20) Lenhardt, J. M.; Ong, M. T.; Choe, R.; Evenhuis, C. R.; Martinez, T. J.; Craig, S. L. Trapping a Diradical Transition State by Mechanochemical Polymer Extension. *Science* **2010**, *329*, 1057−1060.

(21) Saha, S.; Bruening, M. L.; Baker, G. L. Facile Synthesis of Thick Films of Poly(methyl methacrylate), Poly(styrene), and Poly(vinyl pyridine) from Au Surfaces. *ACS Appl. Mater. Interfaces* **2011**, *3*, 3042−3048.

(22) Love, J. C.; Estroff, L. A.; Kriebel, J. K.; Nuzzo, R. G.; Whitesides, G. M. Self-Assembled Monolayers of Thiolates on Metals as a Form of Nanotechnology. *Chem. Rev.* **2005**, *105*, 1103−1170.

(23) Zhang, Y.; Lv, B.; Lu, Z.; He, J.; Zhang, S.; Chen, H.; Ma, H. Predicting Au-S Bond Breakage from the Swelling Behavior of Surface Tethered Polyelectrolytes. *Soft Matter* **2011**, *7*, 11496−11500.

(24) Zhu, Y.; Lv, B.; Zhang, P.; Ma, H. Swelling Induced Au-S Bond Breakage is Determined by the Molecular Composition of Surface Tethered Copolymers-Carboxylated Poly(OEGMA-r-HEMA). *Chem. Commun.* **2011**, *47*, 9855−9857.
(25) Jiang, H.; Xu, F.-J. Biomolecule-Functionalized Polymer Brushes. *Chem. Soc. Rev.* **2013**, *42*, 3394−3426.
(26) Fu, L.; Chen, Y.; Ma, H. Solidified Liquid Layer Model Expands the Application Fields of Quartz Crystal Microbalance. *Macromol. Rapid Commun.* **2012**, *33*, 735−741.
(27) Ma, H.; Wells, M.; Beebe, T. P.; Chilkoti, A. Surface-Initiated Atom Transfer Radical Polymerization of Oligo(ethylene glycol) Methyl Methacrylate from a Mixed Self-Assembled Monolayer on Gold. *Adv. Funct. Mater.* **2006**, *16*, 640−648.
(28) Breen, T. L.; Fryer, P. M.; Nunes, R. W.; Rothwell, M. E. Patterning Indium Tin Oxide and Indium Zinc Oxide Using Microcontact Printing and Wet Etching. *Langmuir* **2001**, *18*, 194−197.
(29) Salaita, K.; Wang, Y.; Mirkin, C. A. Applications of Dip-Pen Nanolithography. *Nat. Nanotechnol.* **2007**, *2*, 145−155.
(30) In the section of "The influence of film area on ABB", the final ratio of OEGMA to HEMA units in polymer brushes was 1:3, so $T_{critical,dry}$ = 53−57 nm as discussed in the Introduction.
(31) Edmondson, S.; Frieda, K.; Comrie, J. E.; Onck, P. R.; Huck, W. T. S. Buckling in Quasi-2D Polymers. *Adv. Mater.* **2006**, *18*, 724−728.
(32) Singamaneni, S.; McConney, M. E.; Tsukruk, V. V. Swelling-Induced Folding in Confined Nanoscale Responsive Polymer Gels. *ACS Nano* **2010**, *4*, 2327−2337.
(33) Amin, I.; Steenackers, M.; Zhang, N.; Beyer, A.; Zhang, X.; Pirzer, T.; Hugel, T.; Jordan, R.; Gölzhäuser, A. Polymer Carpets. *Small* **2010**, *6*, 1623−1630.